Taylor & Francis
Taylor & Francis Group

Predictive pre-cooling of thermo-active building systems with low-lift chillers

N. T. Gayeski,[1,2,*] P. R. Armstrong,[3] and L. K. Norford[4]

[1]*Building Technology Program, Massachusetts Institute of Technology, Rm 5-418, 77 Massachusetts Ave., Cambridge, MA 02139, USA*

[2]*KGS Buildings, LLC, Cambridge, MA, USA*

[3]*Mechanical Engineering Program, the Masdar Institute of Science and Technology, Abu Dhabi, United Arab Emirates*

[4]*Department of Architecture, Massachusetts Institute of Technology, Cambridge, MA, USA*

[*]*Corresponding author e-mail: gayeski@mit.edu*

This article describes the development and experimental validation of a data-driven model predictive control algorithm that optimizes the operation of a low-lift chiller, a variable-capacity chiller run at low pressure ratios, serving a single zone with a thermo-active building system. The predictive control algorithm incorporates new elements lacking in previous chiller pre-cooling control optimization methods, including a model of temperature and load-dependent chiller performance extending to low-pressure and part-load ratios and a data-driven zone temperature response model that accounts for the transient thermal response of a concrete-core radiant floor thermo-active building system. Data-driven models of zone and concrete-core thermal response are identified from monitored zone temperature and thermal load data and combined with an empirical model of a low-lift chiller to implement model predictive control. The energy consumption of the cooling system, including the chiller compressor, condenser fan, and chilled-water pump energy, is minimized over a 24-h look-ahead moving horizon using the thermo-active building system for thermal storage and radiant distribution. A generalized pattern-search optimization over compressor speed is performed to identify optimal chiller control schedules at every hour, thereby accomplishing load shifting, efficient part-load operation, and cooling energy savings. Results from testing the system's sensible cooling efficiency in an experimental test chamber subject to the typical summer week of two climates, Atlanta, GA, and Phoenix, AZ, show sensible cooling energy savings of 25% and 19%, respectively, relative to a high efficiency, variable-speed split-system air conditioner.

Introduction

A low-lift cooling system combines a low-lift chiller (a variable-capacity chiller that operates efficiently at low pressure ratios and over a wide capacity range), radiant cooling with variable-speed distribution, predictive pre-cooling of thermal energy storage (TES), and a dedicated outdoor air system (DOAS) for ventilation and dehumidification to achieve low-energy cooling (Jiang et al. 2007; Armstrong et al. 2009a, 2009b; Katipamula et al. 2010). Efficient operation of a low-lift chiller

Received January 4, 2011; accepted October 25, 2011

Nicholas T. Gayeski, PhD, is Research Affiliate at Massachusetts Institute of Technology and Partner at KGS Buildings. **Peter R. Armstrong, PhD**, is Associate Professor. **Leslie K. Norford, PhD** is Professor.

HVAC&R Research, 18(5):1–16, 2012.
ISSN: 1078-9669 print / 1938-5587 online
DOI: 10.1080/10789669.2012.643752

is enabled through predictive pre-cooling of TES, such as a thermo-active building system (TABS). The chiller operates at lower average lift conditions through lower part-load operation overnight and higher chilled-water temperatures for radiant TABS distribution, and thus higher average chiller efficiencies (Gayeski et al. 2010). Extensive simulation of low-lift cooling systems has shown significant potential annual cooling energy savings in a range of climates and building types relative to conventional variable air volume (VAV) systems (Armstrong et al. 2009a, 2009b; Katipamula et al. 2010). For typical buildings, Katipamula et al. (2010) found that simulated annual cooling energy savings relative to VAV systems with conventional two-speed chillers ranged from 37% to 84%, depending on the climate and building type. These simulations assume ideal thermal storage, not real thermal storage such as TABSs.

This article describes the development of a data-driven model predictive control algorithm that accounts rigorously for the TABS transient response and optimizes control of a low-lift chiller used to pre-cool TABS-TES. The pre-cooling control algorithm has been applied to a low-lift chiller serving an experimental test chamber with a TABS radiant floor subjected to two typical summer week climate conditions. The algorithm integrates for the first time a temperature- and load-dependent low-lift chiller performance model with data-driven temperature response models of zone *and a TABS* to optimize sensible cooling system performance through predictive pre-cooling control. The performance and optimization of the DOAS component of a low-lift cooling system can be treated separately, assuming that the DOAS includes its own efficient variable-capacity direct expansion (DX) cooling or other efficient dehumidification separate from the low-lift chiller plant serving the TABS.

The sensible cooling energy performance of the low-lift cooling system with optimized pre-cooling of TABSs is compared to that of a high-efficiency, variable-capacity split-system air conditioner serving the same experimental chamber. These two systems have been chosen for experimental comparison as a subset of the eight system configurations simulated by Armstrong et al. (2009a, 2009b) and Katipamula et al. (2010) comprising all combinations of the following subsystem alternatives:

- a two-speed chiller or variable speed chiller,
- a VAV system or a radiant cooling system with a DOAS, and
- TES with predictive pre-cooling control or no TES and no pre-cooling control.

The variable-capacity split-system air conditioner serving the experimental test chamber is similar to the radiant system with variable-speed chiller and passive TES simulated in this previous research because the fan power of the ductless indoor unit is very small (0.1076 W/L/s [0.05 W/CFM] at high speed).

The research presented here advances the state of the art in two important ways. First, a predictive *TABS pre-cooling* control algorithm is developed to control a low-lift chiller that accounts for the TABS temperature response and its effect on chiller efficiency. Second, a low-lift cooling system is tested experimentally for the first time.

Literature review

Predictive control to pre-cool TES has been studied with a variety of system configurations and operating modes. Topics addressed in the literature include pre-cooling of discrete-active TES, such as ice-storage or stratified chilled-water tanks; instrinsic-passive storage, such as building thermal mass; and intrinsic thermo-active TES, such as a TABS.

Traditional, intrinsic-passive TES applications use conventional cooling equipment such as VAV systems to sub-cool zones and thereby pre-cool building thermal mass from zone air (Eto 1984; Brandemuehl et al. 1990; Conniff 1991). TABS thermal storage utililizes pipe embedded in the building structure to actively charge building thermal mass, which then passively absorbs heat from occupied zones over the day subject to the temperature response of both the zone system and TABS.

Pre-cooling strategies for intrinsic-passive TES often involve a schedule of zone temperature set-points and/or pre-cooling rates for conventional VAV or other air handling systems. The schedules attempt to reduce peak power demand or minimize energy cost or consumption. Peak load reduction by passive pre-cooling of TES through scheduling zone set-points has been extensively studied (Snyder and Newell 1990; Rabl and Norford 1991; Keeney and Braun 1996; Braun and Chaturvedi 2002; Braun and Lee 2006; Roth et al. 2009) but the impact of pre-cooling on chiller performance has not. Henze et al. (1997, 2004) optimized zone set-points and a discrete-active TES pre-cooling control

schedule based on two constant coefficients of performance (COPs) to account for the difference in chiller COP during chilled-water and ice-making operation. Then studies appeared regarding the impact of forecasting uncertainty (Henze et al. 1999), adaptive thermal comfort criteria (Henze et al. 2007), energy and demand charges and other utility rate structures (Braun 2007; Henze et al. 2008), and simplified optimization methods (Henze et al. 2010). However, none of the research above accounts rigorously for the temperature- and load-dependent performance of variable-speed chillers that are highly efficient at part load, which may greatly enhance the energy efficiency of pre-cooling strategies (Jiang et al. 2007; Armstrong et al. 2009a, 2009b; Katipamula et al. 2010).

Braun (1990) and Kintner-Meyer and Emery (1995) presented pre-cooling control optimization methods in which the temperature and part-load-dependent performance of conventional chillers were taken into account. Chiller performance is a function of condensing, evaporating, and part-load conditions; however, the modeled chiller performance did not reflect more efficient part-load and low-pressure-ratio operation now possible with high-efficiency variable-capacity chillers. Armstrong et al. (2009a, 2009b) presented an approach in which semi-empirical component-based models of low-lift variable-capacity chillers are used to optimize the control of a low-lift chiller serving idealized TES in simulation. Armstrong et al. (2009a) simulated low-lift cooling systems in five climates and reported significantly more potential cooling energy savings than previous pre-cooling strategies. largely because of improved low-lift part-load chiller performance. However, those authors did not fully account for the transient response of intrinsic-active TES, such as a TABS, and its impact on the performance of the low-lift chiller.

Effective control of cooling through TABSs and its potential for cooling energy savings are an open area of investigation (Doebbler et al. 2010). TABSs are most effective in buildings with high-performance envelopes and moderate loads (Brunello et al. 2003; Lehmann et al. 2007) and require careful humidity control, such as through a DOAS (Adlam 1948; Mumma and Shank 2001), and concrete surface or chilled-water temperature control to prevent condensation. Olesen et al. (2002) presented a study of control concepts for TABSs that focused primarily on the timing and duration of cooling the concrete core relative to thermal comfort and pumping energy consumption. Recent developments in TABS control have focused on room temperature feedback and pulse-width modulated pump operation to further reduce pumping energy and improve comfort (Güntensperger et al. 2005; Gwerder et al. 2009). None of the foregoing TABS control strategies accounts for the performance of the chiller serving the TABS, and only recently has simplified zone temperature feedback been incorporated into the control (Gwerder et al. 2009).

Low-lift predictive pre-cooling control for TABS

This article presents a model-based predictive control algorithm for a TABS served by low-lift chillers that incorporates zone and TABS thermal response models as well as a low-lift chiller performance model into the control. TABSs are particularly appropriate for low-lift cooling systems because of the following:

- TABSs require only moderate temperature chilled water;
- TABSs have high thermal storage efficiency, defined as the magnitude of stored cooling energy extracted for cooling relative to the magnitude of cooling energy delivered to storage; and
- TABSs operate with very low transport energy costs.

A framework for optimal control of low-lift chillers to pre-cool TABS is presented that determines an optimal control schedule at each hour, looking ahead 24 hours. A 24-h look ahead is common in pre-cooling control algorithms, because average chiller efficiency can be enhanced by load shifting relative to the diurnal cycle of outdoor temperature and cooling loads (Krarti et al. 1999). In some cases, especially in the case of discrete TES where charging and discharging rates can be controlled and when demand charges are taken into account, longer prediction horizons may be appropriate. However, when TES consists only of a TABS, the prediction horizon is limited in practice by the capacity of TABS-TES and limited control over discharge rates for stored cooling energy.

The control algorithm presented here minimizes cooling energy consumption (or cost) over 24 hours by controlling chiller compressor speed and condenser fan speed in a near-optimal way. The objective function includes a model of a variable-capacity

chiller, presented in Gayeski et al. (2010), that accounts for the temperature- and load-dependent chiller power consumption and cooling rate. It also includes transfer function models of concrete-core temperature response and zone temperature reponse (Seem 1987; Armstrong et al. 2006a, 2006b). The objective function for the model predictive control optimization can be described mathematically as follows:

$$\arg\min_{\omega} J = \sum_{N=1}^{24} (r_N P_N + \varphi PO_N + PE_N), \quad (1)$$

where J is the sum over 24 hours of the cooling system energy consumption (or cost), a penalty for operative temperatures outside of a comfort range, and a penalty for chiller evaporating temperatures below a low temperature threshold. The variables are as follows:

- r_N is a weighting factor set to one to minimize energy consumption or a utility rate to minimize cost;
- P_N is the average power input to the cooling system during hour N, which is a function of outdoor temperature, evaporating temperature (which is a function of concrete-core temperature), and the optimal compressor and condenser fan speeds at N;
- φ is a weighting factor to penalize excursions from an allowable operative temperature region;
- PO_N is a penalty function of zone operative temperatures $T_{o,N}$ at time N, which is a function of current and past thermal loads and temperatures as described below; and
- PE_N is a penalty function of chiller evaporating temperature relative to a low temperature threshold, which prevents predicted controls that would cause freezing.

Models for chiller performance and zone and concrete-core temperature response implicit in Equation 1 are described in the following sections.

Chiller performance model

The cooling system energy consumption P_n includes the energy consumption of the water circulation pump and the low-lift chiller serving the TABS and is given by the following equation:

$$P_N = P_{pump,N} + P_{chiller,N}(T_{x,N}, T_{e,N}, \omega_N, f(T_{x,N}, T_{e,N}, \omega_N)), \quad (2)$$

where $P_{pump,N}$ is the energy consumption of the chilled-water pump over the hour N, and $P_{chiller,N}$ is a regression-based curve-fit model of the power consumption of a low-lift chiller.

The chiller power consumption at hour N, $P_{chiller,N}$, is shown in Equation 3. It is a tri-cubic in evaporating temperature T_e, outdoor air temperature T_x, and compressor speed ω, with five additional terms involving condenser fan speed f.

$$P_{chiller,N} = \begin{pmatrix} c_1 + c_2 T_e + c_3 T_x + c_4 \omega + c_5 T_e^2 \\ + c_6 T_x^2 + c_7 \omega^2 + c_8 T_z T_e + c_9 T_e \omega \\ + c_{10} T_x \omega + c_{11} T_e^3 + c_{12} T_x^3 + c_{13} \omega^3 \\ + c_{14} T_e^2 T_x + c_{15} T_e^2 \omega + c_{16} T_x^2 T_e \\ + c_{17} T_x^2 \omega + c_{18} \omega^2 T_e + c_{19} \omega^2 T_x \\ + c_{20} T_e T_x \omega + c_{21} f + c_{22} f^2 \\ + c_{23} f T_e + c_{24} f T_x + c_{25} f \omega \end{pmatrix}_N \quad (3)$$

The coefficients of this model can be determined for variable-capacity chillers through regression based on physics-based performance simulations or measurements of actual chiller performance. Models of the same form as Equation 3, but with different coefficients, can be identified to represent cooling capacity $QC_{chiller,n}$ and electric input ratio (EIR) $EIR_{chiller,n}$ as functions of T_e, T_x, ω, and f. These models have been identified in a calibrated test stand for the same manufacturer and model of variable-capacity chiller/heat pump used in the following described experiments. The identified models for Equation 3 fit measured power, cooling rate, and EIR with model accuracies of 5.5% or less down to pressure ratios of 1.2 (Gayeski et al. 2010). Models identified from measured data should not be assumed to be valid outside of the range of conditions tested experimentally. Curve-fit models, suitable for integration in a predictive control algorithm, can also be identified from physics-based models of chillers (Zakula 2010) that may be generated by simulating a particular system configuration given the capacity and configuration of each component and a suitable range of operating conditions.

Zone and concrete-core temperature response models

The presence of T_e in Equations 2 and 3 requires that evaporating temperature be estimated at each time step of the 24-h optimization. The prediction of T_e may be based on engineering calculations or data-driven models relating the chilled-water

supply or return temperatures and the chilled-water flow rate to chiller evaporating temperature at specific operating conditions. For a given chiller with a given evaporator water flow rate, a given compressor speed, and a given closed-loop superheat control algorithm, T_e is directly related to chilled-water return temperature T_{chwr} (Armstrong et al. 2009b).

Gayeski (2010) showed that T_{chwr} can be predicted based on past cooling rates, return water temperatures, and concrete-core temperature T_{cc} using a simple second-order transfer function model for T_{chwr}, equivalent to a second-order thermal RC model, as a function of cooling rate $QC_{chiller}$ and concrete-core temperature T_{cc} measured at top-of-tube elevation. This model is shown in Equation 4:

$$T_{chwr,N} = \sum_{n=N-2}^{N-1} a_n T_{chwr,n} + \sum_{n=N-2}^{N} b_n T_{cc,n} + \sum_{n=N-2}^{N} c_n QC_{chiller,n}. \quad (4)$$

An application of comprehensive room transfer function (CRTF) models (Seem 1987; Armstrong et al. 2006b) can be used to predict zone operative temperature and concrete-core temperature T_{cc} in Equation 4 (Gayeski 2010). A CRTF is a combination of two or more conduction transfer functions (Stephenson and Mitalas 1967, 1971) that predicts cooling loads from zone temperatures, outdoor temperatures, and thermal loads (Armstrong et al 2006a; Seem 1987). Temperature CRTFs are complementary to CRTFs and predict zone temperatures from cooling rates, outdoor temperatures, and thermal loads, rather than predicting cooling loads. Physical constraints on the coefficients of temperature CRTF models have been presented by Armstrong et al. (2006b) that resulted in causal, stable, and generally more reliable models than black-box models.

In low-lift predictive pre-cooling of the TABS, the operative temperature T_o is predicted from the following M^{th}-order temperature CRTF model:

$$T_{o,N} = \sum_{n=N-M}^{N-1} o_n T_{o,n} + \sum_{n=N-M}^{N} p_n T_{x,n} + \sum_{n=N-M}^{N} q_n T_{a,n} + \sum_{n=N-M}^{N} r_n QI_n + \sum_{n=N-M}^{N} s_n QC_{chiller,n}. \quad (5)$$

The temperature of the concrete-core T_{cc} is predicted from a similar temperature-CRTF model:

$$T_{cc,N} = \sum_{n=N-M}^{N-1} d_n T_{cc,n} + \sum_{n=N-M}^{N} e_n T_{x,n} + \sum_{n=N-M}^{N} f_n T_{a,n} + \sum_{n=N-M}^{N} g_n QI_n + \sum_{n=N-M}^{N} h_n QC_{chiller,n}. \quad (6)$$

In Equations 5 and 6, T_o is the zone operative temperature, T_{cc} is the concrete-core temperature, T_x is the outdoor air temperature, T_a is an adjacent zone temperature (multiple zones in general but in the experiment only one), QI is the internal heat load, and $QC_{chiller}$ is the cooling rate delivered by the low-lift chiller. The lowercase letters are CRTF coefficients for each variable at each time step n into the past.

The operative temperature $T_{o,N}$ and concrete-core temperature $T_{cc,N}$ at the next time step N are predicted from measurements of each variable at the previous timesteps $N - M$ to $N - 1$ and forecasts of exogenous variables at timestep N. A number, $Z - 1$, of adjacent zones may be incorporated by creating Z CRTF models and solving for Z zone operative temperatures. The choice of chiller compressor speed at each hour of the 24-h look-ahead control schedule determines the cooling rate and, thus, zone operative temperature, concrete-core temperature, chilled-water temperature, evaporating temperature, chiller power consumption, and chiller cooling rate at each hour of the next day.

Operative temperature comfort penalty

The second term in Equation 1 accounts for zone operative temperature comfort constraints. The operative temperature penalty is given by the following equation:

$$\varphi PO_N = \begin{cases} \varphi((T_{o,\min} + 0.5) - T_{o,N})^2 & T_{o,n} \le T_{o,\min} + 0.5 \\ 0 & T_{o,\min} + 0.5 < T_{o,n} < T_{o,\max} - 0.5 \\ \varphi((T_{o,N} - (T_{o,\max} - 0.5))^2 & T_{o,n} T_{o,\max} - 0.5 \end{cases}; \quad (7)$$

$T_{o,\min}$ and $T_{o,\max}$ are the minimum and maximum allowable operative temperatures, and $T_{o,N}$ is the operative temperature at the current timestep N. Operative temperatures outside of and within 0.5°C (0.9°F) of the comfort bounds based on ASHRAE Standard 55 (ASHRAE 2007) are penalized, with a quadratically increasing penalty moving away from the comfort bounds so that the derivatives are continuous at the boundaries. The weight φ penalizes operative temperature excursion relative to power consumption. A choice for φ greater than the minimum chiller power consumption at a given speed will cause an operative temperature penalty greater than the cost of running the chiller during that hour when operative temperature exceeds comfort bounds by 0.5°C (0.9°F). The relative humidity of the zone is not included in the pre-cooling objective function because humidity is controlled separately by a DOAS and does not take part in the pre-cooling optimization.

Chiller operational constraint penalty

The last term in the objective function, PE_n, is a constraint on the evaporating temperature T_e of the refrigerant to prevent control actions (cooling rates) at future time steps that would cause the chiller to freeze. The constraint $T_{e,\min}$ can be chosen conservatively to prevent T_e below 1°C (1.8°F). The evaporating temperature penalty function is as follows:

$$PE_n = \begin{cases} 0 & T_e(T_{chwr,n}) > T_{e,\min} \\ INF & T_e(T_{chwr,n}) \leq T_{e,\min} \end{cases}. \qquad (8)$$

Predictive pre-cooling control optimization method

In the previous section, an objective function was defined for the pre-cooling control algorithm, which contains penalties for energy consumed by the cooling system, operative temperatures outside of a defined comfort region, and low evaporating temperatures. This section describes how the objective function in Equation 1 is minimized to optimize the chiller control over a 24-h look-ahead schedule.

Each hourly cost component of the objective function is evaluated sequentially from hour 1 to 24. At a given timestep, the choice of compressor speed will determine the cooling rates $QC_{chiller}$ and $P_{chiller}$ and, along with exogenous variable forecasts, will determine T_o, T_{cc}, T_{chwr}, and T_e at the next time step. The power consumption and cooling rate of the chiller are non-linear functions of T_x, T_e, ω, and f, where T_e depends on previous choices of compressor speed.

The chiller capacity and power consumption are discontinuous at the minimal compressor speed, at which they drop to zero. This discontinuity in power consumption, representing the finite minimum capacity of the chiller and its auxiliary equipment, precludes the use of gradient-based optimization methods. Optimization methods that do not require calculation of a gradient, such as direct search, generalized pattern search (GPS), genetic algorithms, and simulated annealing, were considered for application to this problem. In practice, GPS (Torczon 1997; Lewis and Torczon 1999, 2000, Audit and Dennis 2003) was found to identify near-optimal solutions within a few minutes on a standard personal computer.

The GPS seeks optimal compressor speeds for every timestep N in the 24-h-ahead schedule of chiller operation, resulting in a 24-dimensional search space. The compressor speed at each hour can take the values of $\omega = 0$ Hz (off), and anywhere within its range of operation, $\omega_{\min} < \omega < \omega_{\max}$ and the resulting sequence of current and past ω_N determine the evolution of $P_{chiller}$, $QC_{chiller}$, T_o, T_e, and T_{cc} at the next timestep. Beginning with a guess at an initial point in the 24-dimensional grid of compressor speeds, the GPS evaluates, or polls, the objective function at a grid of points created with a given grid step size surrounding the initial guess for a more optimal solution. If a more optimal solution is identified, the grid is polled again around that new point. The grid step size is increased, up to the maximum step size; each time a more optimal point in the grid is identified to ensure that basins of convergence far from the current point are tested. If a more optimal grid point is not found at the largest grid step size, the GPS continues around the current point with a smaller grid step size, down to a minimum step size to find the most optimal solution in that region of convergence. The GPS stops when no more optimal points can be found at the smallest grid step size.

A detailed explanation of the GPS algorithm is included Matlab's Global Optimization Toolbox: User's Guide (Mathworks 2010), and more information can be found in Torczon (1997), Lewis and Torczon (1999, 2000), and Audit and Dennis (2003). Unlike the gradient-based method, GPS can search different basins of convergence from an initial guess within, for example, a basin of a local optimum.

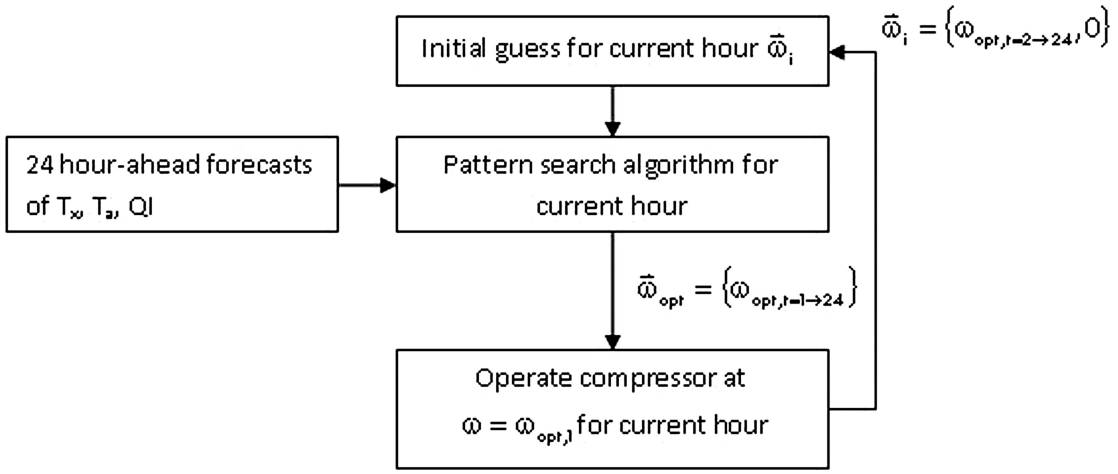

Figure 1. Closed-loop optimization of compressor speed for low-lift cooling of the TABS with pattern search.

However, GPS does not guarantee convergence to a global optimum.

A flowchart of the GPS algorithm implemented for optimizing the daily schedule of compressor speeds is shown in Figure 1. An initial guess of 24 compressor speeds $\vec{\omega}_n$ is made at each hour, which may be based on the previous hour's result. The GPS algorithm is run to identify an optimal schedule of compressor speeds $\vec{\omega}_{opt}$ for the next 24 hours. At each iteration of the pattern search, Equations 2 through 8 are applied to calculate $P_{chiller}$, $QC_{chiller}$, T_o, T_{cc}, and T_{chwr}. The pattern search may be repeated at each hour in a closed-loop optimization (Henze et al. 2004) with updated forecasts of outdoor air temperature T_x, adjacent zone air temperature T_a, and internal loads QI at each hour. The optimal compressor speed for the first hour of the optimization, computed by the GPS, determines the chiller compressor speed for the next hour, after which the process is repeated.

Experimental implementation of low-lift predictive pre-cooling of TABS

The predictive control algorithm described above has been implemented on a low-lift chiller serving a concrete-core TABS in an experimental test chamber. The primary objective of these experiments was to experimentally test the effectiveness of the predictive pre-cooling control algorithm. A secondary objective was to compare the sensible cooling energy performance of the pre-cooled TABS radiant cooling system with a case similar to one of the simulated basecase systems studied by Katipamula et al. (2010). Of the eight other cases simulated, the radiant system with a variable-capacity chiller is closest to the variable-capacity, split-system air conditioner used as the experimental base case. The simulation and experimental base cases are similar in the lack of pre-cooling TES, transport energy costs, and chiller performance.

Experimental facilities

An existing experimental test facility (Yang 1999; Kobayashi 2001) was adapted for testing low-lift cooling experimentally. The lab includes two chambers, one test chamber representing a typical office zone with one exterior wall and another climate chamber used to simulate climate conditions outside the exterior wall. The test chamber has dimensions of roughly 3.66 m by 5.18 m by 2.44 m (12 ft by 17 ft by 8 ft). The walls of both chambers are heavily insulated with a thermal resistance of about 5.3 m^2-K/W (30 ft^2-F-hr/BTU). A partition wall separates the test and climate chambers, which contains three large double-pane windows with a thermal resistance of approximately 0.27 m^2-K/W (1.53 ft^2-F-hr/BTU). The surrounding environment is a 6 m by 12 m (20 ft by 40 ft) high-bay laboratory space maintained at 20°C to 24°C (68°F to 75.2°F).

The climate chamber temperature is controlled by a constant-volume air handling unit with the return air temperature set-point adjusted at every hour to follow the typical summer week of a typical meteorological year (TMY) weather file. The test

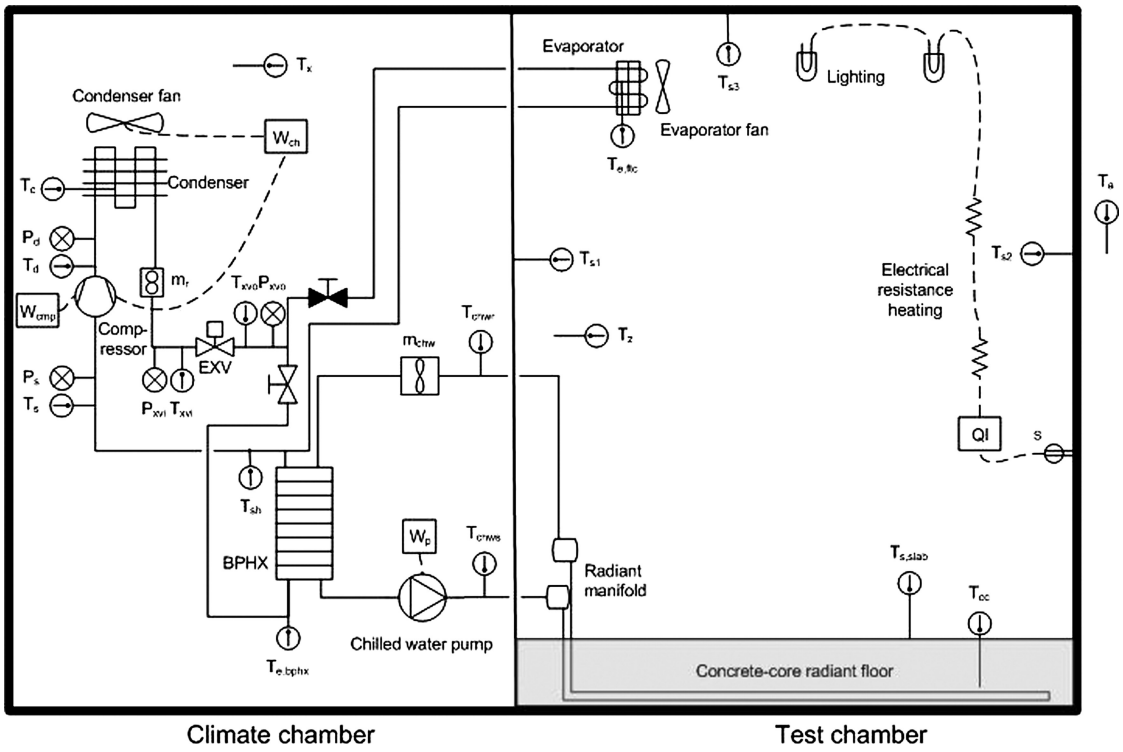

Figure 2. Schematic elevation of the experimental test chamber and cooling system.

chamber has a modular floor constructed to mimic a TABS using an aluminum-faced subfloor, polyethylene (PEX) pipe, and 14.6-cm (5.75-in.) concrete pavers. Chilled water supplied by the low-lift chiller cools the bottom of the concrete pavers via the aluminum-faced subfloor, resulting in a thermal lag between the time cooling is delivered and heat is absorbed from the test chamber. The air-cooled variable-capacity low-lift chiller is installed in the climate chamber. The chiller was constructed using an off-the-shelf variable capacity split-system air conditioner condensing unit, described in Gayeski et al. (2010), with a rated seasonal energy efficiency ratio (SEER) of 16 BTU/Wh (4.69 Wth/W_e). To convert this condensing unit to a low-lift chiller, a refrigerant loop through a brazed-plate heat exchanger (BPHX) was added along with means to control the compressor at low speeds to enable low-lift operation. A schematic of the variable capacity chiller, the climate and office test chamber, and associated instrumentation is shown in Figure 2. Lighting and electrical resistance heating elements simulate typical office internal gains.

There are six parallel water loops in the radiant floor, each made of 12.7-mm (0.5-in.) PEX pipe, designed to minimize pressure drop in the TABS radiant floor. The pipe spacing of 30.5 cm (12 in.) is large and results in unnecessarily low chilled-water temperatures and will be modified in future work. The chilled-water pump serving the radiant floor was operated at a constant speed of 0.13 L/s (2.1 GPM) with a power consumption of approximately 145 W/L/s (9.1 W/GPM). A variable-speed pump may further improve the low-lift cooling system efficiency but will also increase model and optimization complexity.

Data-driven temperature response model identification

The coefficients of Equations 4 through 6, which predict zone operative temperature, TABS concrete-core temperature, and chiller evaporating temperature, must be identified from monitored data. In the case of the experimental test chamber, the temperatures and loads in Equations 4 through 6 refer to measured variables from sensors installed in the office test chamber and climate chamber shown in Figure 3. T_o, T_x, T_a, and T_{cc} are calculated from surface and air temperatures measured using 24-gauge

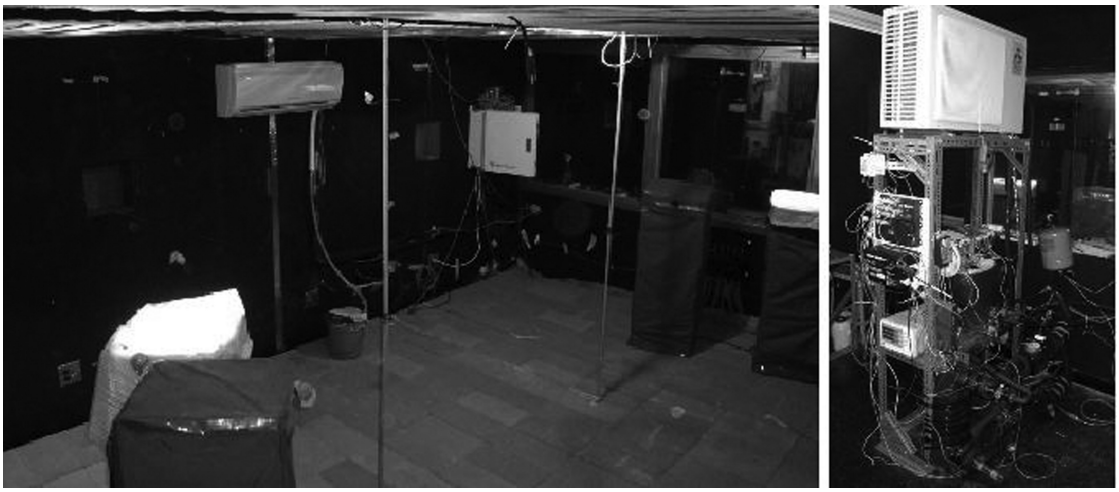

Figure 3. Left: Test office chamber with concrete radiant floor, simulated internal loads, and a conventional split-system air conditioner indoor unit. Right: Low-lift chiller in the climate chamber.

special-limits thermocouples. Thermocouples connected to a given multiplexer agree with each other to within 0.01 K (0.018°F) + 0.4%. Terminal reference sensors are accurate to 0.4 K over −25°C to 50°C (0.7°F over −13°F to 122°F) and have been found to agree within 0.1 K (0.2 F) at room temperature. *QI*, the internal heat rate to the zone, is measured using Wattnode power meters with a rated accuracy of 0.5%. The cooling rate delivered by the chiller, $QC_{chiller}$, is calculated from chilled-water flow rate measured with an Omega FTB8007B flow meter with an acurracy of 1.5%, and supply and return temperatures, T_{chws} and T_{chwr}, are measured using special-limits 1/16″ sheathed thermocouple probes.

M^{th}-order models of zone operative temperature and concrete-core temperature can be identified from at least 4 days of training data using multi-variable regression. A specific sample training dataset used to estimate the parameters of the models given by Equations 4 through 6 for the experimental test chamber is shown in Figure 4. For this test chamber, an eighth-order model, with 30-min sampling intervals, provided the best 24-h-ahead prediction accuracy (Gayeski 2010) when applied to separate validation datasets. For a variety of

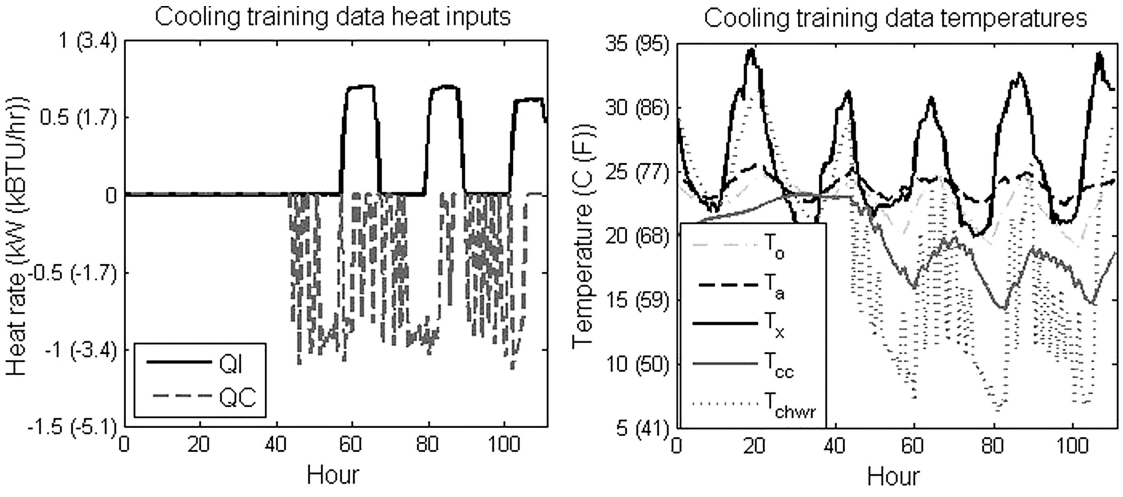

Figure 4. Sample temperature response model training data.

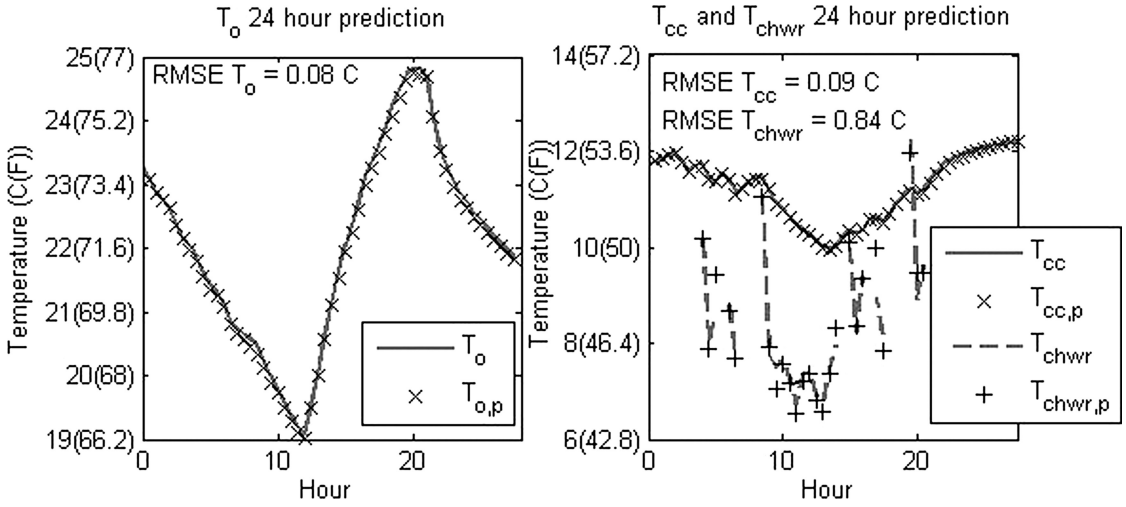

Figure 5. Twenty-four-hour-ahead forecasts relative to measured data of test chamber operative temperature (left) and concrete core and return water temperature (right).

validation datasets spanning different cooling rates, internal load schedules, and climate conditions, operative temperature and concrete-core temperature could be predicted over a 24-h look ahead with root-mean-square error (RMSE) of less than 0.5°C (0.9°F) (Gayeski 2010). A second-order model for chilled-water return temperature was identified from the same training data based on measured cooling rates and the TABS concrete-core temperature T_{cc}. This model had an RMSE of less than 1°C (1.8°F) across all validation datasets. From the prediction of chilled-water return temperature, the evaporating temperature at the chiller can be calculated using the approach temperature of the BPHX. The 24-h-ahead forecasts of operative temperature, concrete-core temperature, and chilled-water return temperature are compared to measured values in Figure 5. Using logged data from a building automation system, the coefficients of these models could be updated continuously in a full-scale building. The model order and sampling intervals that lead to the most accurate data-driven temperature response models will differ for different buildings and can be selected based on validation data prediction accuracy.

Experimental test procedure

The sensible cooling performance of the low-lift cooling system with predictive pre-cooling of a TABS was compared to that of a variable-capacity split-system air conditioner in the test chamber. The split system represents one of the cases with no pre-cooling simulated by Katipamula et al. (2010). Two pairs of experiments were performed where these systems were subjected to the typical summer week of the TMY weather for Atlanta, GA, at Hartsfield-Jackson airport and for Phoenix, AZ, at Deer Valley airport, August 24–30 in both cases. The internal heat rate for the Atlanta tests represented standard performance loads for lighting and internal equipment gains (Gayeski 2010; Katipamula et al. 2010), but high occupant loads, for a total of 36.6 W/m^2 (11.6 BTU/hr-ft^2) at peak load and a load schedule representative of a small commercial office. High-performance loads for lighting and internal equipment gains (Gayeski 2010; Katipamula et al. 2010), but again high occupant loads, were applied in the Phoenix tests at a heat rate of 21.5 W/m^2 (6.8 BTU/hr-ft^2) at peak load. The total loads, including high occupant loads, are oversized to better match the chiller capacity and allow a suitable range for chiller operation.These loads were measured with electric power meters as denoted in Figure 2. The adjacent zone temperature T_a in Equations 4 and 5, represents the external lab temperature and was held nearly constant. In these experiments QI, T_x, and T_a are controlled and are thus predictable inputs to the models and optimization algorithms. In practice, these variables will have error and uncertainty in prediction that must be taken into account (Henze and Krarti 1999).

Because the TABS radiant floor provides only sensible cooling, the relative humidity of the chamber was kept as low as possible to avoid latent

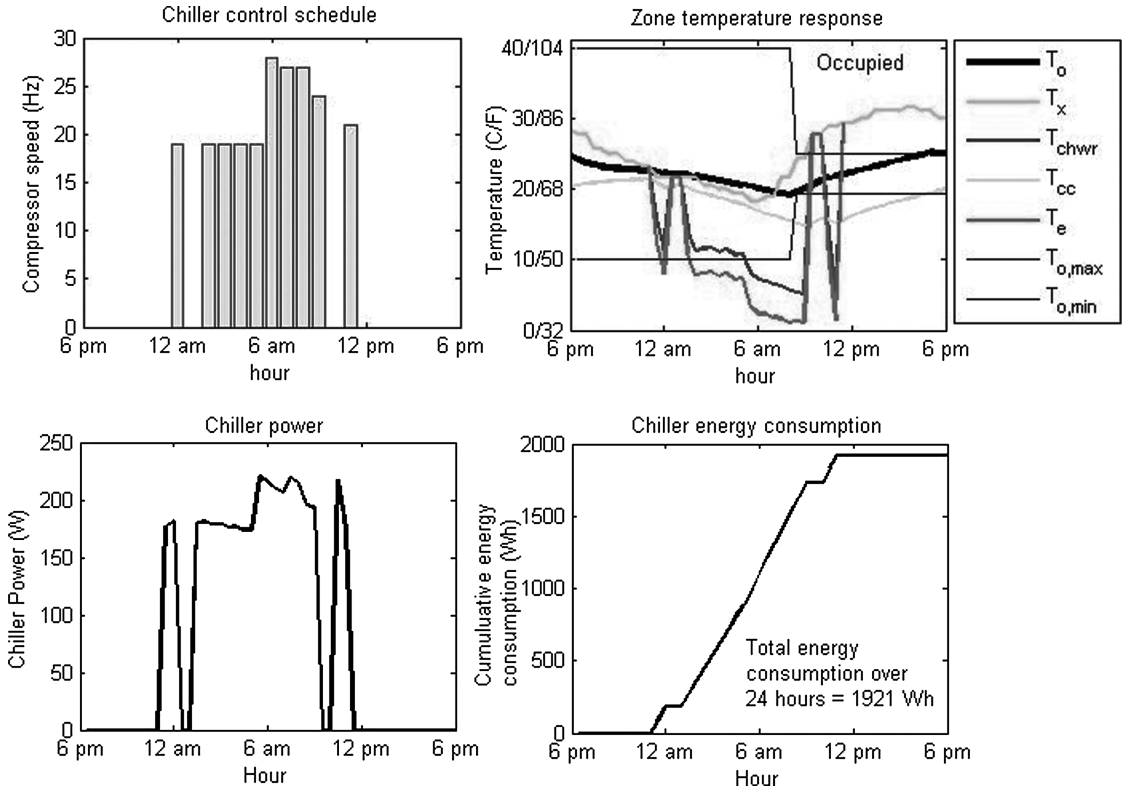

Figure 6. Typical low-lift pre-cooling optimization for TABS from an experimental test chamber (color figure available online).

cooling. As discussed above, latent cooling would be performed separately by a DOAS with separate DX cooling or efficient dehumidification. Any condensed water produced during testing with the conventional indoor unit was collected and weighed in order to adjust cooling energy to the sensible cooling basis.

The following process was employed to evaluate energy and thermal performance of the low-lift cooling system relative to the variable-capacity split-system air conditioner.

- The climate chamber was controlled at each hour to achieve typical summer week temperatures.
- The internal loads were controlled to deliver the load schedules defined above to the test chamber.
- The low-lift cooling system with the TABS was operated for one week, including one weekend, maintaining operative temperature between 19.5°C and 25°C (67°F and 78°F) (ASHRAE 2007) while occupied.
- The variable-capacity split-system air conditioner was operated for one week, including one weekend, using conventional thermostatic control to achieve the same daily average temperature as the low-lift cooling system.

Figure 6 illustrates a typical sequence of optimal compressor speeds for a 24-h look-ahead schedule produced by the predictive control algorithm. Compressor speeds for each of the 24 hours into the future are shown at the top left. The predicted operative temperature T_o, concrete-core temperature T_{cc}, return water temperature T_{chwr}, and evaporating temperature T_e for this schedule are shown at the top right. The predicted chiller power consumption $P_{chiller}$ is shown at bottom left, and the cumulative energy consumption is shown at bottom right. For the hour following this optimization, the low-lift chiller would be operated at the first predicted optimal compressor speed, which is 0 Hz (or off) in the case below, and the predictive control optimization would be repeated at the next hour, with the previous hour's schedule as an initial guess for the GPS.

The sequences illustrated in Figure 6 demonstrate certain aspects of predictive control for low-lift cooling with TABS. First, the most efficient time to perform most of the cooling is at night and during

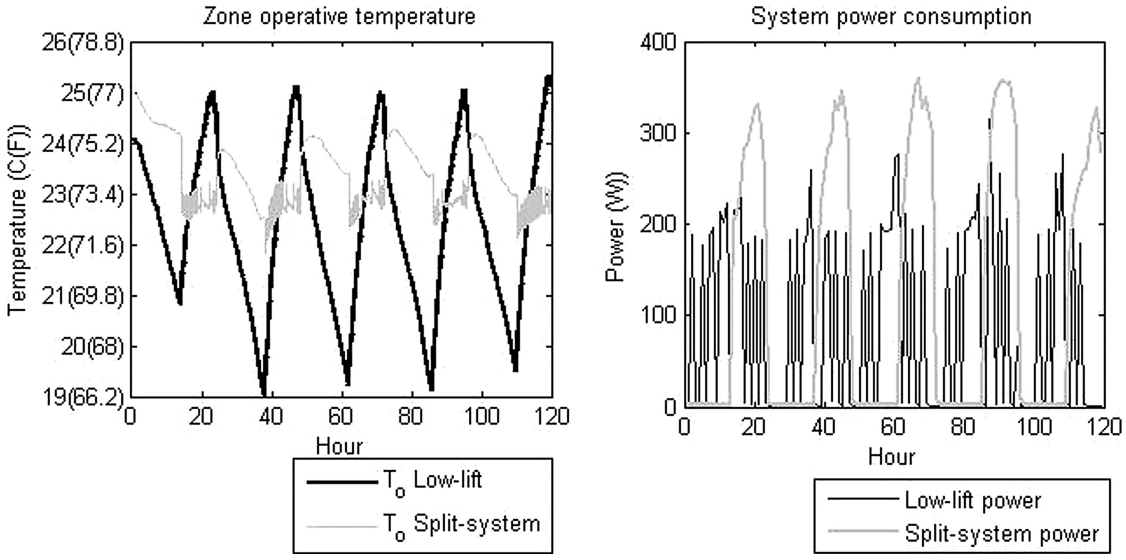

Figure 7. Operative temperature and system power consumption of the low-lift cooling system and a split-system air conditioner subject to Atlanta typical summer week conditions and standard efficiency loads.

the early morning hours under low-lift conditions. Second, the chiller runs at low part loads more of the time, which is also more efficient. Third, because the efficiency of the chiller depends on evaporating temperature, the compressor cycles off at times to avoid low evaporating temperatures and provide higher chiller efficiency while operating at the low end of its capacity range.

This predictive control algorithm operates continuously during the course of each experiment, updating chiller compressor speed, fan speed, and chilled-water pump availability at each hour. The tests described here were used to measure the performance of the algorithm under typical summer week conditions. The data-driven temperature response model is not guaranteed to be valid under operating conditions not previously observed. However, the model may be updated continuously and over time be trained for a broad range of thermal inputs. Non-ideal cases, such as rapid or high frequency changes in internal gains, were not tested experimentally. These types of inputs, if the models had not yet been trained for them, would lead to greater error in model predictions.

Energy and thermal performance

Figure 7 shows the zone operative temperature response and the system power consumption for the Atlanta test for the low-lift cooling system and the variable-capacity split-system air conditioner spanning the week of occupied operation. The intial temperature conditions for the split- and low-lift systems differ because the systems were tested under steady-periodic behavior, operating under the same system for the previous week and achieving a typical Monday start-up condition. Two characteristics of low-lift cooling are apparent in the pattern of energy consumption: (1) the cooling rate is distributed over time, allowing the chiller to run at lower speeds and lower part loads and (2) cooling is delivered to the TABS overnight when lower condensing temperatures are possible.

The average daily mean operative temperature difference between the low-lift cooling system tests and the split-system tests was small: 0.3°C (0.54°F) for the Atlanta tests and −0.5°C (−0.9°F) for the Phoenix tests. The main difference in thermal environment provided by the systems is the slow temperature rise of the conditioned zone for low-lift cooling with TABS. High convective internal loads cause significant increases in zone operative temperature relative to the radiant cooling surface. This is a recognized limitation of radiant cooling system and TABSs (Meierhans 1996; Koschenz and Dorer 1999), which may preclude the application of the TABS, and low-lift cooling with a TABS, from low performance buildings and buildings with high internal loads.

Results similar to those shown in Figure 7 were observed for testing under Phoenix conditions with high-performance internal loads, except that the

Table 1. Energy performance (±0.5%) of low-lift cooling system relative to a variable-capacity split-system air conditioner.

	Atlanta, August 24–30			Phoenix, August 24–30		
Performance metric	Split system	Low lift	Difference	Split system	Low lift	Difference
Energy (Wh_e)	14,465	10,982	−25%	21,153	17,205	−19%
Energy consumption (Wh_e)[a] with latent cooling deducted	14,053	10,982	−22%	21,153	17,205	−19%
Average pressure ratio	1.91	1.70	−11%	2.12	1.99	−6%

[a]The latent energy consumption can only be estimated for split-system operation based on measurement of the mass of water condensed. The low-lift system also may have performed some latent cooling.

lower internal convective heat rate provided by high-performance internal loads led, despite higher outdoor temperatures, to a lower operative temperature rise. A comparison of the energy performance of the two cooling systems in each of the two climates is shown in Table 1. The table shows relative performance in terms of energy consumed and average pressure ratio, representative of internal lift, for the period of each test.

The results show that low-lift cooling system sensible cooling energy savings can be significant relative to a high-efficiency split-system air conditioner that uses the same variable-capacity compressor-condensing unit but with no pre-cooling. The measured energy consumption of the experimental low-lift cooling system was 25% less than the split-system under Atlanta conditions and 19% less under Phoenix conditions. Accounting, conservatively, for latent cooling performed by the split system reduces the savings to 22% for Atlanta.

The closest system configurations modeled by Katipamula et al. (2010) are not directly comparable to the systems tested experimentally; however, it is of interest to evaluate the experimental savings relative to the most similar simulated savings for the same typical summer weeks in Atlanta and Phoenix and similar internal loads. The simulated case with a variable-speed chiller and radiant distribution is closest to the variable-capacity split system tested experimentally due to its low fan power and the absence of latent cooling. The simulated sensible cooling energy savings of a low-lift cooling system with variable-speed chiller and pre-cooling of ideal TES relative to a comparable system without pre-cooling TES in Atlanta was 26%. For Phoenix, with high-performance loads, the simulated sensible cooling energy savings for the typical summer week were 29%. Differences between simulated savings and experimental savings are expected for several reasons; the simulated TABS included an ideal TES (pre-cooling case), a different chiller performance map, and a lower (per unit capacity) evaporator to zone thermal resistance. Neither the experimental nor the simulated savings presented above include the additional total cooling savings relative to conventional VAV systems, which could be provided by efficient latent cooling by a DOAS (Katipamula et al. 2010).

The limitations of the experimental facility should be considered when interpreting the experimental results. The following factors caused lower low-lift cooling system performance than possible in theory:

- an oversized chiller is used because a compressor small enough to match the small test chamber was not available;
- the internal loads are oversized to better match the chiller capacity but cause a greater operative temperature rise and zone temperatures closely coupled to convective loads and, consequently, less load shifting;
- the single-story test chamber allows cooling energy losses through the floor, which would not occur in a multi-story building; and
- the chilled-water pipe spacing of 30 cm (12 in.) dictated by standard radiant heating components is, in retrospect, too large for low-lift cooling applications with a TABS. A smaller pitch of 10–15 cm (4–6 in.) typical of radiant cooling applications would result in higher chilled-water temperatures, higher evaporating temperatures, and more efficient low-lift cooling system operation.

Although the results presented above reflect a comparison of a low-lift cooling system with only one other system configuration in two climates, they are a useful benchmark against simulations conducted in previous research (Armstrong et al. 2009a, 2009b; Katipamula et al. 2010). Further research is required to adapt and implement this control scheme in alternative low-lift cooling system configurations, incorporate DOAS control of latent loads, and compare performance to other systems. These comparisons, however, are not trivial. Building simulation tools are still not fully capable of simulating receding horizon model-predictive control algorithms that include deteailed models of cooling system performance and building temperature response, especially with thermally massive TABSs. Experimental comparisons are possible but expensive, time-consuming, and subject to uncertainties that simulations neglect.

Summary

This article presents a data-driven, model-based predictive control algorithm for low-lift chillers serving a concrete-core TABS and its implementation in an experimental test chamber. Temperature- and load-dependent curve-fit chiller performance models and zone operative temperature and concrete-core temperature CRTF models are incorporated into a predictive control optimization algorithm. The algorithm determines optimal sequences of compressor and condenser fan speeds for each 24-h period to minimize low-lift cooling system energy consumption while maintaining thermal comfort. Closed-loop optimization has been successfully implemented in which the optimal chiller control schedule is determined at every hour based on the latest measured zone temperatures and internal loads. In practice, these hourly updates would also consider new forecasts of weather and internal loads.

An experimental implementation of the predictive control algorithm for low-lift cooling with a TABS demonstrated significant sensible cooling energy savings, consistent with previous simulation results for low-lift cooling systems (Katipamula et al. 2010). The experimental base system was a high-efficiency split system served by the same outdoor unit (compressor, condenser, EXV, and power electronics) employed by the low-lift chiller. The experiments for low-lift cooling with the TABS under Atlanta conditions with standard performance loads showed 25% sensible cooling energy savings, and under Phoenix summer conditions with high-performance internal loads, it was 19%. Latent cooling energy has not been included because low-lift cooling systems utilize a separate DOAS for dehumidification, as described by Armstrong et al. (2009a, 2009b).

Discussion

The predictive control strategy presented here has been developed primarily for single-zone low-lift predictive pre-cooling of TABS with predictable loads. A number of important additions and revisions must be made to this control strategy for implementation in a broader context. First, the algorithm should be revised to include solar loads, measured or estimated occupant behaviors, and multi-zone control and supply of the TABS. The inclusion of a variable-speed chilled-water pump serving the TABS and the chiller will also be important, as it may allow for further improvements in chiller efficiency and control.

A strategy that combines pre-cooling of TABS with direct cooling of zones is likely to achieve the best balance of system efficiency and comfort control. This will also ameliorate the effects of errors in forecasts of exogenous variables, such as internal or solar gains and outdoor temperature, and errors in predictions of zone temperatures by the data-driven models. Therefore, another important advance will be to incorporate the option for direct cooling of the zone, not through TABS but through conventional air-side evaporators, large heat exchanger fan coil units, or radiant cooling panels.

It is worth reiterating that the objective in this work has been to minimize the *energy* needed to run the cooling system. To minimize *cost*, one needs to modify the rate function r_N in Equation 1 using real-time or time-of-use rates and add demand charges to the objective function. Experience has shown consistently that the resulting percent savings in operating cost are substantially larger than the energy savings percentages (minimum based on flat rate) for most utility customers.

Improvements to the experimental implementation of low-lift cooling with TABS presented in this article will improve both the energy and thermal performance of the system. These improvements include better load matching, decreased chilled-water pipe pitch, additional under-slab insulation to better

mimic multi-story performance, and optimization of the BPHX.

Acknowledgments

The authors wish to acknowledge the Masdar Institute of Science and Technology for support of this research. They are grateful for the support and advice of members of the Mitsubishi Electric Research Laboratory and the Pacific Northwest National Laboratory. Nicholas Gayeski is also thankful for the support of the Martin Family Society of Fellows for Sustainability. Thanks to Heejin Cho and Pacific Northwest National Laboratory for providing the intermediate files needed to conduct the modeled savings comparison and to Kurt Keville and the MIT Solar Decathlon team for the split system.

References

Adlam, T. 1948. *Radiant Heating*. New York, NY: The Industrial Press.

Armstrong, P.R., W. Jiang, D. Winiarski, S. Katipamula, and L.K. Norford. 2009a. Efficient low-lift cooling with radiant distribution, thermal storage, and variable-speed chiller controls—Part II: Annual energy use and savings. *HVAC&R Research* 15(2):402–32.

Armstrong, P.R., W. Jiang, D. Winiarski, S. Katipamula, L.K. Norford, and R.A. Willingham. 2009b. Efficient low-lift cooling with radiant distribution, thermal storage, and variable-speed chiller controls—Part I: Component and subsystem models. *HVAC&R Research* 15(2):366–400.

Armstrong, P.R., S.B. Leeb, and L.K. Norford. 2006a. Control with building mass—Part I: Thermal response model. *ASHRAE Transactions* 112(1).

Armstrong, P.R., S.B. Leeb, and L.K. Norford, 2006b. Control with building mass—Part II: Simulation. *ASHRAE Transactions* Vol. 112(1).

ASHRAE. 2007. ANSI/ASHRAE Standard 55-2007, thermal environmental conditions for human occupancy. Atlanta, GA: American Society of Heating, Refrigerating, and Air-Conditioning Engineers.

Audit, C., and J.E. Dennis. 2003. Analysis of generalized pattern searches. *SIAM Journal on Optimization* 13(3):889–903.

Brandemuehl, M.J., M.J. Lepoer, and J.F. Kreider. 1990. Modeling and testing the interaction of conditioned air with building thermal mass. *ASHRAE Transactions* 96(2):871–5.

Braun, J.E. 1990. Reducing energy costs and peak electrical demand through optimal control of building thermal storage. *ASHRAE Transactions* 96(2):876–88.

Braun, J.E. 2007. Impact of Control on Operating Costs for Cool Storage Systems with Dynamic Electric Rates. *ASHRAE Transactions* 113(2): 343–354.

Braun, J.E., and N. Chaturvedi. 2002. An inverse gray-box model for transient building load prediction. *HVAC&R Research* 8(1):73–97.

Braun, J.E., and K.H. Lee. 2006. Assessment of demand limiting using building thermal mass in small commercial buildings. *ASHRAE Transactions* 112(1):547–58.

Brunello, P., M.D. Carli, M. Tonon, and R. Zecchin. 2003. Applications of heating and cooling thermal slabs for different buildings and climates. *ASHRAE Transactions Symposia*, 2003:637–46.

Conniff, J.P. 1991. Strategies for reducing peak air-conditioning loads by using heat storage in the building structure. *ASHRAE Transactions* 97(1):704–9.

Doebbler, I.M., M. Moore, and M. Deru. 2010. Radiant slab cooling for retail. *ASHRAE Journal* 52(12):28–39.

Eto, J.H. 1984. Cooling strategies based on indicators of thermal storage in commercial building mass. *Annual Symposium on Improving Building Energy Efficiency, College Station, TX, August 14–15*.

Gayeski, N. 2010. Predictive pre-cooling control for low-lift radiant cooling using building thermal mass. Doctoral dissertation, Massachusetts Institute of Technology, Cambridge, MA.

Gayeski, N., T. Zakula, P.R. Armstrong, and L.K. Norford. 2010. Empirical modeling of a rolling-piston compressor heat pump for predictive control in low-lift cooling. *ASHRAE Transactions* 117(2):ML-11-023.

Güntensperger, W., M. Gwerder, A. Haas, B. Lehmann, F. Renggli, and J. Tödtli. 2005. Control of concrete core conditioning systems. *8th REHVA World Congress for Building Technologies(CLIMA 2005), Lausanne, Switzerland, October 10–12*.

Gwerder, M., J. Tödtli, B. Lehmann, V. Dorer, W. Güntensperger, and F. Renggli. 2009. Control of thermally activated building systems (TABS) in intermittent operation with pulse width modulation. *Applied Energy* 86:1606–16.

Henze, G., R.H. Dodier, and M. Krarti. 1997. Development of a predictive optimal controller for thermal energy storage systems. *International Journal of HVAC&R Research* 3(3):233–64.

Henze, G., C. Felsmann, and A. Florita. 2008. Optimization of building thermal mass control in the presence of energy and demand charges. *ASHRAE Transactions* 114(2):75–84.

Henze, G., C. Felsmann, and G. Knabe. 2004. Evaluation of optimal control for active and passive building thermal storage. *International Journal of Thermal Sciences* 43(2):173–83.

Henze, G., A. Florita, M. Brandemuehl, C. Felsmann, and H. Cheng. 2010. Advances in near-optimal control of passive building thermal storage. *Journal of Solar Energy Engineering* 132:021009.

Henze, G., and M. Krarti. 1999. The impact of forecasting uncertainty on performance of a predictive optimal controller for thermal energy storage systems. *ASHRAE Transactions* 105(1):553–61.

Henze, G.P. 2003. Impact of real-time pricing rate uncertainty on the annual performance of cool storage systems. *Energy and Buildings* 35:313–25.

Henze, G.P., J. Pfafferott, S. Herkel, and C. Felsmann. 2007. Impact of adaptive comfort criteria and heat waves on optimal building thermal mass control. *Energy and Buildings* 39:221–35.

Jiang, W., D.W. Winiarski, S. Katipamula, and P.R. Armstrong. 2007. Cost-effective integration of efficient low-lift

base-load cooling equipment. PNNL-17157. Pacific Northwest National Laboratory. Richland, WA.

Katipamula, S.K., P.R. Armstrong, W. Wang, N. Fernandez, H. Cho, W. Goetzler, J. Burgos, R. Radhakrishnan, and C. Ahlfeldt. 2010. Cost-effective integration of efficient low-lift baseload cooling equipment FY08 final report. PNNL-19114. Pacific Northwest National Laboratory. Richland, WA.

Keeney, K., and J.E. Braun. 1996. A simplified method for determining optimal cooling control strategies for thermal storage in building mass. *International Journal of HVAC&R Research* 2(1):59–78.

Kintner-Meyer, M., and A.F. Emery. 1995. Optimal control of an HVAC system using cold storage and building thermal capacitance. *Energy and Buildings* 23:19–31.

Kobayashi, N. 2001. Floor-supply displacement ventilation system. Master's thesis, Massachusetts Institute of Technology, Cambridge, MA.

Koschenz, M., and V. Dorer. 1999. Interaction of an air system with concrete core conditioning. *Energy and Buildings* 30:139–45.

Krarti, M., G. Henze, and D. Bell. 1999. Planning horizon for a predictive optimal controller for thermal energy storage systems. *ASHRAE Transactions* 105(2).

Lehmann, B., V. Dorer, and M. Koschenz. 2007. Application range of thermally activated buildings systems tabs. *Energy and Buildings* 39(2007):593–8.

Lewis, R.M., and V. Torczon. 1999. Pattern search algorithms for bound constrained minimization. *SIAM Journal on Optimization* 9(4):1082–99.

Lewis, R.M., and V. Torczon. 2000. pattern search methods for linearly constrained minimization. *SIAM Journal on Optimization* 10(3):917–41.

Liu, M., and D.E. Claridge. 1998. Use of calibrated HVAC system models to optimize system operation. *Journal of Solar Energy Engineering* 120.

MathWorks. 2010. *Matlab Global Optimization Toolbox 3: User's Guide*. Natick, MA.

Meierhans, R.A. 1996. Room air-conditioning by means of overnight cooling of the concrete ceiling. *ASHRAE Transactions* 102(1):693–7.

Mumma, S., and K. Shank. 2001. Achieving dry outside air in an energy-efficient manner. *ASHRAE Transactions* 107(1): 1–9.

NIST. 2009. NIST reference fluid thermodynamic and transport properties database (REFPROP): Version 8.0. NIST standard reference database 23.

Olesen, B.W., K. Sommer, and B. Duchting. 2002. Control of slab heating and cooling systems studied by dynamic computer simulations. *ASHRAE Transactions* 108(2): 698–707.

Rabl, A., and L.K. Norford. 1991. Peak load reduction by preconditioning buildings at night. *International Journal of Energy Reseach* 15:781–98.

Roth, K., J. Dieckmann, and J. Brodrick. 2009. Using off-peak precooling. *ASHRAE Journal* March 2009. http://findarticles.com/p/articles/mi_m5PRB/is_3_51/ai_n32067827/.

Seem, J.E. 1987 Modeling of heat transfer in buildings. PhD thesis, University of Wisconsin, Madison, WI.

Snyder, M.E., and T.A. Newell. 1990. Cooling cost minimization using building mass for thermal storage. *ASHRAE Transactions Research* SL-90-14-3.

Stephenson, D.G., and G.P. Mitalas. 1967. Cooling load calculations by thermal response factor method. *ASHRAE Transactions* 73(1).

Stephenson, D.G., and G.P. Mitalas. 1971. Calculation of heat conduction transfer functions for multi-layer slabs. *ASHRAE Transactions* 77(2):117–26.

Torczon, V. 1997. On the convergence of pattern search algorithms. *SIAM Journal on Optimization* 7(1):1–25.

Yang, X. 1999. Study of building material emissions and indoor air quality. PhD thesis. Massachusetts Institute of Technology, Cambridge, MA.

Zakula, T. 2010. Heat pump simulation model and optimal variable-speed control for a wide range of cooling conditions. Master's thesis. Massachusetts Institute of Technology, Cambridge, MA.

Zakula, T., N.T. Gayeski, P.R. Armstrong, and L.K. Norford. 2011. Variable-speed heat pump model for a wide range of cooling conditions and loads. *International Journal of HVAC&R Research* 17(5):670–91.